First European Conference on Earthquake Engineering and Seismology
(a joint event of the 13th ECEE & 30th General Assembly of the ESC)
Geneva, Switzerland, 3-8 September 2006
Paper Number:

NUEMERICAL–EXPERIMENTAL STUDY OF HIGH DAMPING ELASTOMERS FOR ENERGY DISSIPATING DEVICES

Pablo MATA A[1], Ruben BOROSCHEK K[2], Alex H. BARBAT[3] and Sergio OLLER[4]

SUMMARY

In work the results of a study carried out to characterize the mechanical response of a high damping rubber to be used to design and construct energy dissipating devices and base isolators for controlling strong vibrations in civil engineering structures is presented. A new parametric constitutive model of the rubber is proposed to be employed in the design procedure and structural analysis of passive controlled structures. The parameters of the model are calibrated using experimental results obtained from tests on rubber specimens subjected to different loading paths. The new model is able to reproduce the main dissipative mechanisms as well as axial hardening. The response predicted for the proposed model is compared with these obtained from experimental tests.

1. INTRODUCTION

The mechanical characteristics of rubber including its energy dissipating capacity are strongly dependent on the components of the mixture used and the fabrication process [Soong and Dargush, 1997; Mata and Boroschek 2001]. In general, its mechanical behavior is complex presenting an elastic modulus strongly dependent on the strain level, temperature and loading frequency. Due to these characteristics, the material shows different types of energy dissipating mechanisms, which can go from purely hysteretic, viscous or other [Sommer, 1989; Kojima and Yoshihide 1990]. Additionally, when the material undergoes large strains a noticeable hardening phenomenon appears in the strain-stress response. It is possible to find numerical models of the problem based on the principles of the solid continuous mechanics with appropriate multi–axial constitutive laws for the components of the elastomer [Salomon *et .al*. 1999], but normally they consume a large amount of computer time. Other kind of models are based on fitting parametrical equations to experimental data [Kelly 1988], providing a phenomenological description of the material, and in many cases, of the control devices. This last option presents the advantage of being much more economic in computing time and the calibration of the model can be done directly from loading experimental tests.

Frequently, the practical design of structures with rubber based control systems uses equivalent linear models for the controlling devices [AASHTO, 1991]. This kind of simplified models can induce significant errors in the estimation of the device's response because the elastic modulus and the damping coefficient are constant values for all strain levels and load frequencies [Mata *et. al*. 2005].

[1] Technical University of Catalonia.Edificio C1, Campus Norte UPC. Gran Capitán s/n. Barcelona 08034, Spain.
Email : pmata@cimne.upc.edu
[2] University of Chile, Civil Engineering Department., Blanco Encalada 2002. Santiago, Chile.
Email: rborosch@ing.uchile.cl
[3] Technical University of Catalonia.Edificio C1, Campus Norte UPC. Gran Capitán s/n. Barcelona 08034, Spain.
Email: alex.barbat@upc.edu
[4] Technical University of Catalonia. Edificio C1, Campus Norte UPC. Gran Capitán s/n. Barcelona 08034, Spain.
Email: sergio.oller@upc.edu

This work proposes a new analytical model for rubbers. It is able to simulate the strain hardening for large displacements condition as well as variable elastic modulus. The developed model depends on a set of parameters, which are determined from experimental tests. The model response subjected to several arbitrary loading paths of imposed displacements is compared with experimental data.

2. MECHANICAL CHARACTERIZATION

This part of the work presents the test assembly and the results obtained from tests carried out to characterize the mechanical properties of a high damping rubber. See Figure 1. The force–displacements response of the rubber was obtained for loading paths, which includes sinusoidal cycles with different amplitudes and frequencies and sequences of arbitrary imposed displacements. The dependency between dissipated energy and loading frequency or maximum strain level was studied. An identification of the main dissipative mechanisms is proposed, classifying them in displacement dependent, (hysteretic), and velocity dependent, (viscous).

2.1 Description of the test assembly

Three specimens were tested during the experiments. Each test-piece was composed by five segments, both extreme segments and the central one was made of steel with circular perforations for providing fixation to the test machine. The other two segments were rubber plates of 9 cm^2 of area and 6 mm of thickness. The faces of the rubber plates were adhered to the contiguous steel bodies. By this way, fixing the extreme segments and forcing a displacement in the intermediate one it is possible to develop different loading paths of imposed displacements as it can be seen in Figure 1. The central embolus is connected to the hydraulic actuator of the test machine. The sequence of loading tests was the following:

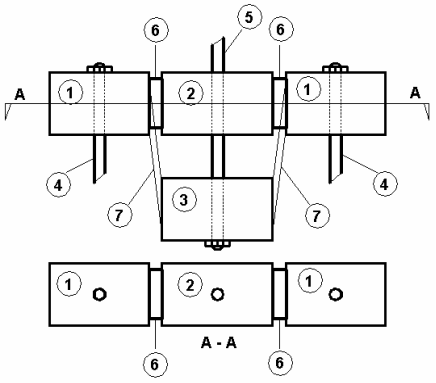

Figure 1: Test Assembly. 1: Fixed steel segments. 2: Movable steel segment. 3: Position of the movable steel segment when a displacement is imposed on the specimen. 4: Fixating bolts. 5: Movable embolus. 6: Rubber plate in original configuration. 7: Deformed rubber specimen.

Symmetric cycles. The specimens were subjected to sinusoidal loading cycles of imposed displacements. The range of maximum applied amplitudes was defined by following values: +/- 10, 20 50, 100, 150, 170 and 200 %, with the following loading frequencies: 1/30, 0,5, 1,0 and 2,0 Hz.

Asymmetric cycles. Sinusoidal cycles of imposed displacement with different maximum and minimum amplitudes were applied. The tests were carried out with a loading frequency of 0.5 Hz. See Table 1 for detailed values of maximum and minimum amplitudes. The objective is to know the rubber behavior for loading cycles displaced from the origin. In Fig. 2a shows samples of the obtained rubber response.

Arbitrary sequences. Finally, two sequences of arbitrary imposed displacements where employed. In Figure 2b it is possible to see the records. The first one corresponds to a sequence of ascending and descending ramps. The second one is a scaled duplicate of the displacement response obtained from a single degree of freedom system with a period of 1 s and 5% of critical damping subjected to the N–S component of El Centro 1945, earthquake record. The purpose of using the last record is to study the rubber response for conditions similar to those expected during an earthquake. See Figure 2b.

Table 1: Asymmetric loading tests.

Test	1	2	3	4	5	6	7	8	9	10	11	12	13	14
Max strain %	200	200	200	200	200	200	200	200	150	150	150	150	150	150
Min strain %	170	150	100	50	20	-20	-50	-100	100	50	20	-20	-50	-100
Test	15	16	17	18	19	20	21	22	23	24	25	26	27	28
Max strain %	100	100	100	100	100	100	50	50	50	50	50	50	50	100
Min strain %	50	20	-20	-50	-100	-150	20	0	-20	-50	-100	-150	-200	50

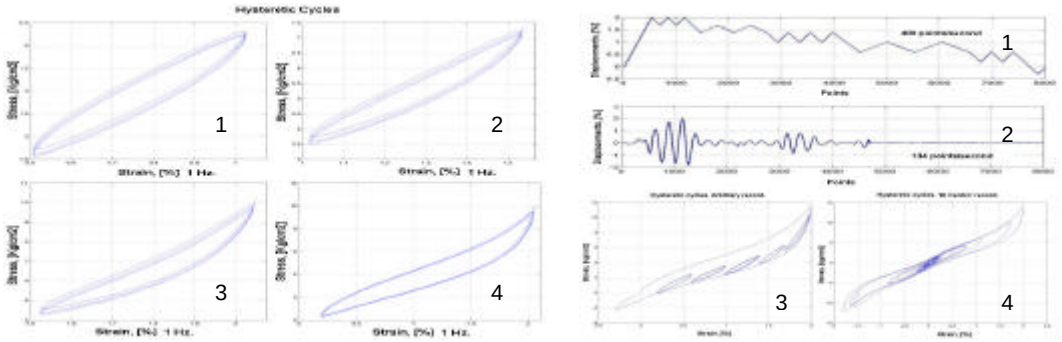

(a) **(b)**

Figure 2: (a) Examples of the results obtained from asymmetric tests (0.5 Hz). 1: 50–100 % max and min strain levels respectively. 2: 100–170 %. 3: 150–200 %. 4: 20–200. (b) 1: Sequence of ramps. 2: Record simulating seismic conditions. 3: Rubber response for the sequence of ramps. 4: Rubber response for the seismic conditions.

2.2 General behavior of the rubber

The general behavior of the rubber can be described as hysteretic with a nonlinear strain–stress relationship. When a test-piece is subjected by first time to sinusoidal cycles, *progressive stiffness degradation* is noticeable. See Figure 3a. The degrading process progress until a stable hysteretic cycle is obtained. Approximately 5 cycles are required before the stabilization. Stiffness degradation can be explained as a transient process of rearrangement of the particles of the material [Salomon *et. al.* 1999; Sommer 1989]. One of the main characteristics of the rubber is a strongly variable elastic modulus for the strain–stress curve. From the symmetric loading tests is possible to identify three different zones:

- *An initial zone* (1), for strains in the range +/-20 %. This zone is characterized tangent to the strain–stress curve higher than in the rest of the strain ranges.
- A *central zone* (2), contained in the range +/- [20–150] %, where the slope tangent decreases.
- An *ending zone* (3), for strain levels higher than 150 % where hardening is present, and the slope of the tangent to the strain–stress curve is increased again.

2.3 Dissipated energy

The energy dissipated in each loading cycle was calculated as the area of the hysteretic cycle [Chopra, 2000]. Figure 4a shows the values obtained for the dissipated energy as function of the maximum strain level for symmetric tests and different loading frequencies. Dissipated energy increases with the strain level due to when higher displacements are imposed, more energy is dissipated. However, the rate of energy dissipation with the strain level is not constant. The slope of the obtained curves is related with the shape of the hysteretic cycles. For low strains the cycles has an approximately elliptic shape as it can be appreciated in Figure 3b, but as strain grows the hysteretic cycles are stretched along the mayor axis of the ellipse. Finally, for high strain levels (> 150 %) axial hardening appears in the response.

In Figure 4b it is possible to see the dependency between dissipated energy and loading frequency. Dissipation increases with frequency. It could indicate that viscous forces are associated with frequency increments. The

results depicted in this figure are normalized, defining the value 1 for the test carried out at 1/33 Hz. This Figure also shows that for all maximum strain levels, the bigger the loading frequency the bigger the dissipated energy. The dissipation rate is maintained constant for damping values higher than 0.5 Hz. In the first range of frequencies (1/33–0.5 Hz) a higher slope of the curve is obtained independently of the strain level. A possible explanation for this could be given by the existence of a component of dissipation purely hysteretic. And therefore, for cuasi static loadings dissipation only depends on maximum strain level.

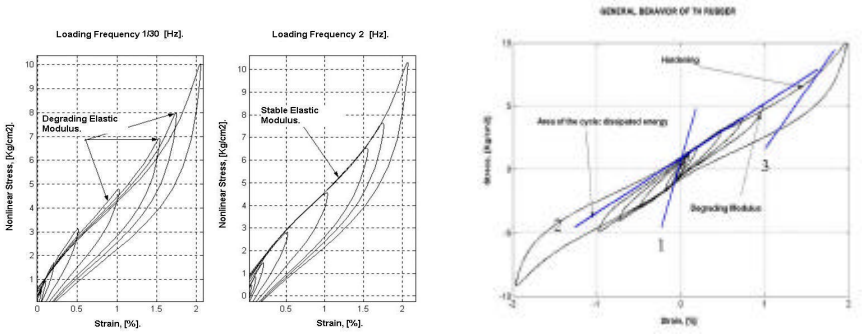

(a) **(b)**

Figure 3: (a) Degradation of the elastic modulus, after a large number of loading cycles the hysteresis became stable. (b) Hysteretic behavior for symmetric loadings. It is possible to appreciate three zones according to the average tangent to the strain–stress curve.

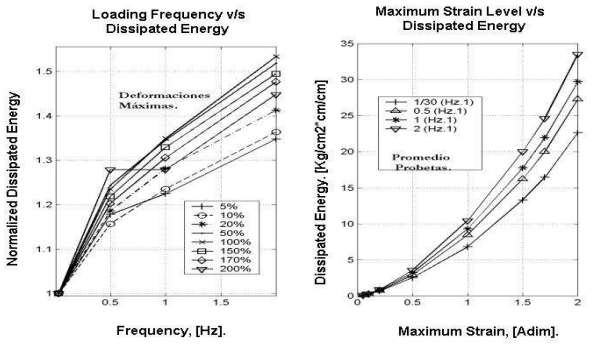

(a) **(b)**

Figure 4: (a) Dissipated energy (normalized) as function of loading frequency. Each curve corresponds to a maximum strain level. (b) Dependency between dissipated energy with maximum strain level. Each curve corresponds to a fixed loading frequency.

Additionally, the *equivalent viscous damping factor* ζ [Chopra, 2000], was calculated for different maximum strain levels and loading frequencies according with the Eqs. (1) and (2).

$$z = \frac{1}{4p}\frac{E_D}{E_{so}}. \tag{1}$$

$$E_{so} = ku_o^2/2. \tag{2}$$

Where E_D is the area of cycle, E_{so} the elastic energy stored in the cycle, k is the average stiffness estimated as the slope of the backbone of the cycle and u_o is the maximum displacement. The values for the factor ζ, for different loading frequencies and strain levels are shown in Figure 5. If the displacement grows the damping factor decreases, which shows that if the maximum strain is increased; the hysteretic cycle losses the elliptic shape presenting an enlargement along the major axis and a bigger stored elastic energy with a minor ratio E_D/E_{so}.

2.4 Behavior for asymmetric loading

From the results of asymmetric loading tests it is possible to conclude that the loading or unloading paths followed by the material are independent on the preview strain history and only are function of the stress–strain state existing in when the strain rate changes of sign. It can be evidenced from Figure 6a where it is possible to see superimposed all the hysteretic cycles for different minimum strain levels, (blue), and a maximum level of

200 %, (black line). In Figure 6b the maximum strain level is 150 %. Additionally, in Figure 6d the results for a maximum strain level of 100 % are depicted. It is possible to conclude that all the hysteretic cycles converge to the enveloping curve of the tests carried out at 200 %. In Figure 6c it is possible to see that the curves generated by tests with a maximum strain level of 100 % superimpose the curves for tests at 150 % concluding that all reloading paths are coincident independently of the maximum strain level reached during the test.

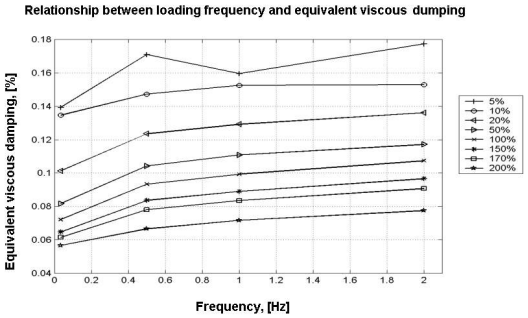

Figure 5: *Equivalent viscous camping factor* for each maximum strain level.

2.5 Rubber Behavior for arbitrary loading

The response of the tests specimens subjected to arbitrary loadings shows the followings characteristics:
The *sequence of ramps* follows the enveloping curve until a strain level of 200 %. After that, several asymmetric cycles are developed at different strain levels. All these cycles are attached to the lower branch of the enveloping curve, see Figure 7. Energy dissipation is obtained in any case. In the case of the *seismic loading* for low strain levels (<50 %) the rubber response is rather stiff, for medium strain levels (50–150 %) the average shear modulus decrease, but the area of the hysteretic cycles is increased. For high strain levels (>150 %) axial hardening became noticeable increasing the stiffness.

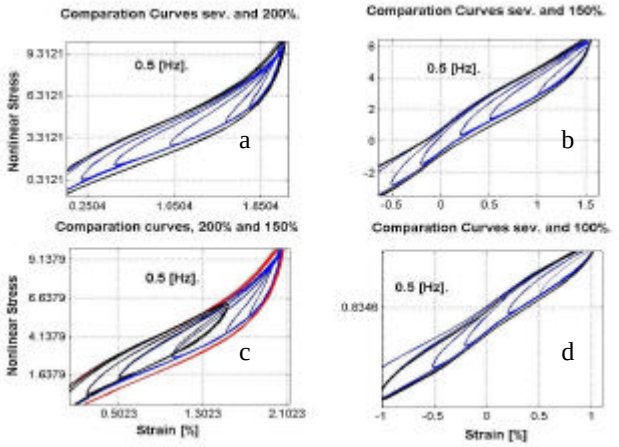

Figure 6: Cycles for different maximum strain levels. All the branches converge to the enveloping curve.

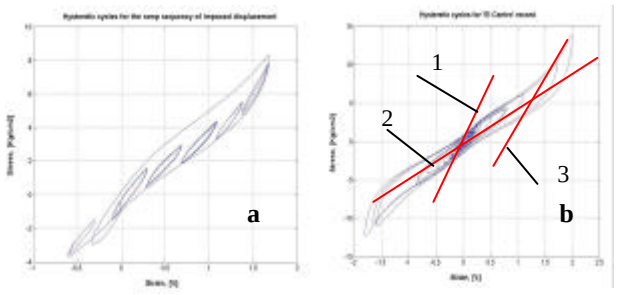

Figure 7: (a) Cycles obtained for the sequence of ramps. Secondary hysteretic cycles are attached to the lower enveloping curve. (b) Rubber response for seismic loading. 1: Average stiffness in low strain level. 2: medium range. 3: large strain level.

3. PROPOSED MODEL

The model proposed for the rubber strain–stress relationship has the following form:

$$s(e,\dot{e},t)=s_1(e,t)+s_2(\dot{e},t)=s_1(e)+0.12\dot{e}. \tag{3}$$

Where s is the total stress, e the strain level, t time, $\dot{e}$ the strain rate, s_1 the hysteretic component of the stress and s_2 is the component depending only on the strain rate. The proposed model uncouples the total stress in viscous and hysteretic components. The parameters of the model have to be calibrated from the test results. The viscous component s_2 is taken equal to $0.12\dot{e}$ according to [Mata *et. al.* 2005]. In agreement with the experimental part the hysteretic component s_1 should be able to simulate *axial hardening* for strain levels over 150 %, *variable shear modulus* and the *initial slope* of a loading or unloading branch should depend only on the point when the material goes from loading to unloading or vice versa. The expression for s_1 is given by

$$s_1=\underbrace{f_2 e(e^{cv},s_{NL})+(f_1(e^{cv})-f_2)e}_{s_{11}}+\underbrace{sgn(\dot{e})5.0(\langle|e|-1.5\rangle)^{1.5}}_{s_{12}}. \tag{4}$$

where s_{11} is the hysteretic part, which is calculated solving the following system of differential equation:

$$s_{11}=k_y(e^{cv},s^{cv})e(e^{cv},s^{cv})+(k_e(e^{cv},s^{cv})-k_y(e^{cv},s^{cv}))e. \tag{5}$$

$$\begin{aligned} &if\ \dot{e}e\geq 0 \quad \rightarrow \quad \dot{e}=(1-\left|\frac{e}{e_y(e^{cv},s^{cv})}\right|^{n(x^{cv},f_{NL}^{cv})})\dot{e} \\ &else \quad \rightarrow \quad \dot{e}=\dot{e}. \end{aligned} \tag{6}$$

being K_y is the post yielding stiffness, K_e the pre yielding stiffness, e the real strain and e represents an internal variable of plastic strain which take a value in the range [$-e_y$, e_y], (e_y is the yielding strain of the material). (x^{cv},f^{cv}) is the point in the strain-stress plane when $\dot{e}=0$. 'n' is the smoothing parameter for transition zone between pre and post yielding branches in the hysteretic cycle [Wilson 1998] (see Figure 8).

The model proposed for the component s_{11} solves the system of Eqs. (5) and (6) having into account that the parameters K_e, K_y, d_y and n, are function of the point where the velocity changes of sign. Therefore, the model is updated when there is a change in the sign of the velocity. By other hand, axial hardening is obtained by mean of adding an appropriated stiffer backbone to component s_{12}. Figure 9 presents a graphic of the proposed function.

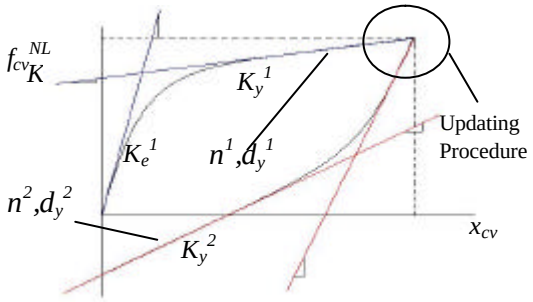

Figure 8: The upper curve is constructed integrating the model for the initial values of the parameters. After the loading–unloading transition has occurred, the parameters of the model are updated.

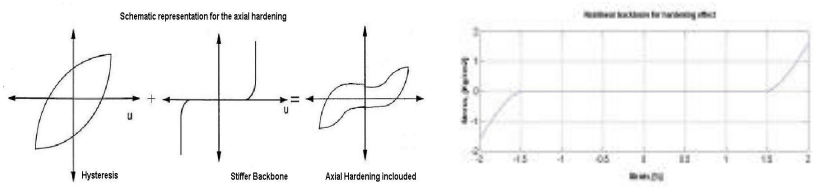

(a) **(b)**

Figure 9: (a) Non linear backbone, s_{11}, added to the hysteretic component s_{22} for including axial hardening. (b) Proposed function for s_{11}.

During the updating procedure it is necessary to know the parameters model expressed as function of the current stress and strain level. Therefore, it is necessary to construct the functions f_1, f_2, f_3 and f_4, Eqs. (4) and (7). Explicit forms for the functions f_1, f_2, f_3, y f_4 have to be determined from experimental data.

$$k_e = f_1(x^{cv}, f_{NL}^{cv}),\ k_y = f_2(x^{cv}, f_{NL}^{cv}),\ d = f_3(x^{cv}, f_{NL}^{cv}),\ n = f_4(x^{cv}, f_{NL}^{cv}). \tag{7}$$

3.1 Pre yielding stiffness function, $K_e = f_1$

This function defines the initial stiffness each time when there is a change in the sign of the strain rate. In this work an additional simplification will be made supposing that f_1 is function only of e^{cv}. The method for determining this function is: For each hysteretic cycle draw *the tangent* to the curve where $\dot{e} = 0$. See Figure 10. Construct the set of pairs composed by each *slope of the tangents* and its corresponding *strain level*. Fit a polynomial to the set of the mentioned points. The obtained polynomial is the function f_1 and for the present work it is given in Eq. (8), employing for seven points obtained from the tests.

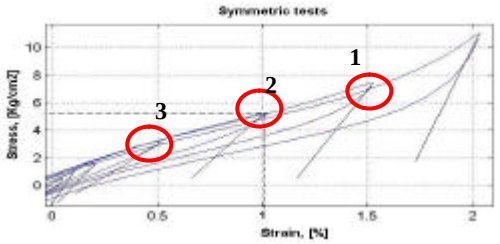

Figure 10: (1, 2, 3): In the circles are highlighted the points where the loading-unloading transition occurs. In each of these points the slope of the tangent to the unloading curve is obtained.

$$f_1(x_{cv}) = -0.14 + 0.95x_{cv} - 2.45x_{cv}^2 + 3.19x_{cv}^3 - 2.25x_{cv}^4 + 0.89x_{cv}^5 - 0.20x_{cv}^6 + 0.04x_{cv}^7. \tag{8}$$

3.2 Post yielding stiffness function, $K_y = f_2$

The value of the post yielding stiffness is maintained constant and equal to the value of the slope of the upper enveloping curve of the test carried out in a maximum strain level of 200 %, due to the fact that all the loading or unloading branches finally converges to the enveloping curve. The function f_2 is defined by Eq. (9).

$$f_2(x_{cv}, Fnl_{cv}) \approx K_y = 3.30. \tag{9}$$

3.3 Yielding strain, $d = f_3$

Having defined the functions f_1 and f_2, the yield displacement function f_3 is constructed intersecting the line with slope f_1 and the enveloping curve with slope f_2. The yield strain is measured from the transition point to the intersecting point. This method for calculating the function f_3 ensures that any loading or unloading branch always will be contained inside the main enveloping hysteretic cycle. The expression for f_3 is given in Eq. (10):

$$f_3(e_{cv}, s_{cv}) \approx f_3(s_{cv}) = \frac{|s_{cv}| - |s_0 - s_{cv}|}{(f_2 - f_1)}. \tag{10}$$

where s_{cv} is the stress in the transition point, s_0 is a parameter calculated evaluating the line with slope f_2 at zero strain level.

3.4 Smoothing function, $n = f_4$

In this work simulations considering a set of 50 values for f_4 in the range [1 5], where carried out to approximate each hysteretic cycle of the symmetric tests. For each simulation one value for the parameter f_4 was chosen according to the following criteria: the differences between the predicted value for the stress and the experimental value were computed. The square root of the absolute modulus of the sum of these differences was chosen as function to be minimized. The parameter f_4, which minimizes this function, is chosen as correct value. The minimizing method allows concluding that the best value for f_4 always is 1.0. Therefore, the smoothing function is given by:

$$f_4(e_{cv}, s_{cv}) \approx f_4 = 1.0. \tag{11}$$

4. COMPARISON BETWEEN NUMERICAL AND EXPERIMENTAL RESULTS

4.1 General behavior of the proposed model.

The model was subjected to a sinusoidal record of imposed displacements with variable amplitude in the range [0.0-2.0] and loading frequency of 0.5 Hz. See Figure 11a. Additionally, to the value of 0.12 Nsm^{-1} for the damping coefficient, two other fictitious values, (0.05 and 0.30), where employed to compare its influence in the response. From Figure 11a it is possible to see that energy dissipation grows as viscous damping coefficient increase. The model shows variable shear modulus and it is possible to distinguish the three zones previously described. For strain levels over 150 % axial hardening is present.

A second set of simulations was carried out to evaluate the capacity of the model to dissipate energy for different loading frequencies. In Figure 11b are depicted the results for a damping coefficient of 0.12 Kgcm. The same input record as in the Fig. 11a was employed, but loading frequencies where 1/33 and 2.00 Hz. In this case it is possible to see the hysteretic part of the dissipated energy for a loading frequency of 1/33 [Hz]. On the side a zoom view of the low strain zone is shown. It is possible to appreciate the initial elliptic shape of the hysteretic cycles. As the strain level grows the ellipse enlarge along its major axis approximating to a rectangular shape.

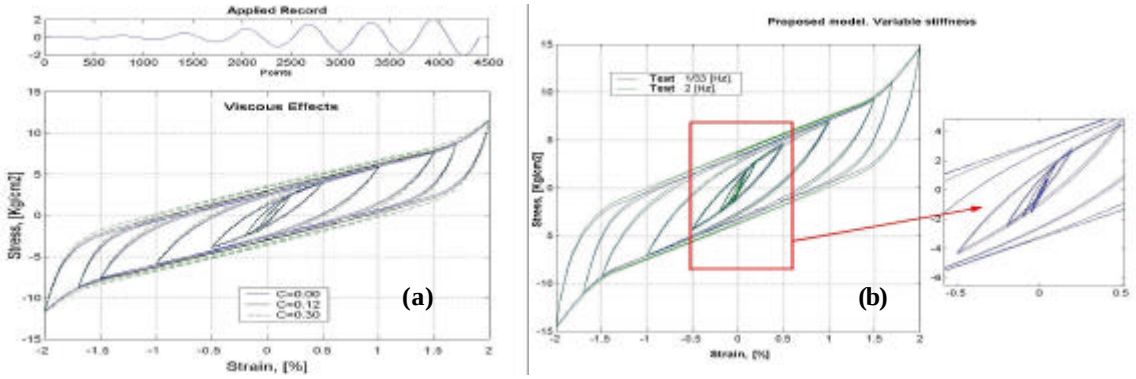

Figure 11: (a) Hysteretic cycles for three damping coefficients. It is possible to appreciate that the energy dissipation grows with the damping coefficient. (b) Different loading frequencies (1/33, 2.00 Hz).

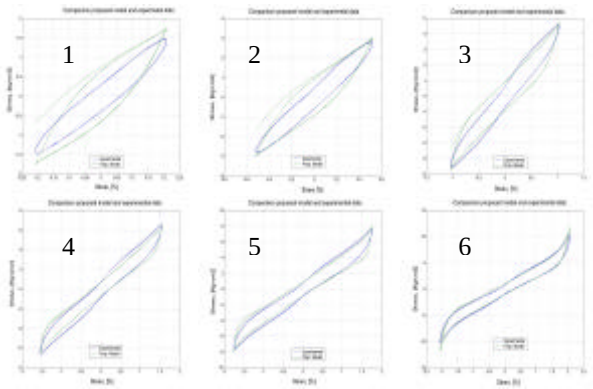

Figure 14: Comparison between the predicted response and experimental data for symmetric sinusoidal tests, 0.5 Hz. Maximum strain levels: 1: 20 %, 2: 50 %, 3: 100 %, 4: 150 %, 5: 170 %, 6: 200 %. A good agreement between predicted and experimental data is obtained.

4.2 Comparison between the proposed model and experimental data

The response model was compared with the experimental data for symmetric tests carried out with loading frequency of 0.5 Hz. Figure 14 shows superimposed in a same picture the predicted and experimental responses. A good agreement is obtained for all strain levels but better fittings are obtained for strain levels over 50 %. The results shown in this figure allows to confirm the capacity of the model to reproduce the rubber behavior including variable stiffness, axial hardening and the changes in the shape of the hysteretic cycles.

4.3 Comparison between the proposed model and experimental data for arbitrary loading tests

Figure 15 shows the results of simulating the rubber response for the seismic loading case. On the left side it is possible to see a good agreement between the hysteretic cycles obtained from numerical simulation and experimental data. The model is able to reproduce variable stiffness and axial hardening. The well fitting is confirmed on the right side of the figure: the predicted stress time history fits the experimental values with a precision of (+/- 5 %).

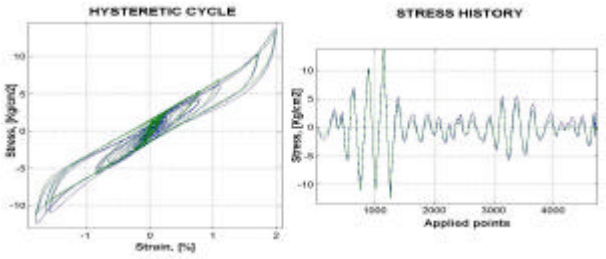

Figure 15: Comparison between numerical simulation and experimental data for the seismic loading case. Left: Hysteretic cycles. A general good agreement is obtained. Right: Stress time history. Blue: experimental record. Green: predicted response.

Finally, it is possible to say that the proposed numerical model is able to reproduce the rubber behavior for an arbitrary loading case.

5. CONCLUSIONS

The mechanical characteristic of a rubber candidate to be base material to develop passive control devices was studied in this work. A set of tests was carried out on test specimens for knowing the rubber response subjected to imposed displacements. The dependency of the response with frequency and strain level was studied. The main dissipative mechanisms were identified grouping them in hysteretic and viscous, according if dissipation is displacement or velocity dependent. The displacement dependent part of the dissipation was studied, concluding that the response of material does not depend on the previous strain history. Among the more remarkable characteristics of the hysteresis are: strongly variable elastic stiffness, axial hardening for strain levels over 150 % and shape changes in hysteretic cycles with strain level. Additionally, a new model for the rubber behavior was proposed, developed and validated. The new model is constructed adding three components: a linear viscous dashpot acting in parallel with a stiffener backbone and a nonlinear hysteretic spring. All the parameters for the components of the proposed model have to be calibrated from experimental data and the corresponding methods are developed in the work. The nonlinear hysteretic spring response is obtained solving a system of differential equations describing the relationship between stress and strain. The model is validated comparing the predicted response with the data obtained from symmetrical and arbitrary tests. In both cases the proposed model is able two reproduce the rubber response with an acceptable precision level.

6. ACKNOWLEDGMENT

This work has been partially supported by: University of Chile, Project FONDECYT nº 1970732; Ministerio de Ciencia y Tecnología, Spain, Project: "Numerical simulation of the seismic behavior of structures with energy dissipation systems" Contract nº: BIA2003 - 08700 - C03 – 02; and the Integrated R&D Project of the EC "LessLoss–Risk Mitigation for Earthquakes and Landslides" funded by the European Commission, Directorate General of Research under the Contract nº GOCE-CT-2003-505448.

7. REFERENCES

AASHTO [1991] *Guide Specifications for base isolation design*. A. Assoc. of State Hwy. and Transp. Officials, Washington, D.C.

Asano, M. Masahiko, H. and Yamamoto, M. [2001] "The Experimental Study on Viscoelastic Material Dampers and the Formulation of Analytical Model", *Proceedings of the Twelve-World Conference on Earthquake Engineering.* Paper nº 1535.

Barbat, A. H., Oller, S. Oñate, E. and Hanganu, A. [1997] "Viscous Damage Model for Timoshenko Beam Structures*", Int. J. Solids Structures*, 34, 3953 - 3976.

Chopra, A. [2000] *Dynamics of Structures: Theory and Applications to Earthquake Engineering* Prentice Hall, Inc. Upper Saddle River, New Jersey, Second Edition.

Kojima, H. and Yoshihide, Y. [1990] "Performance, Durability of High Damping Rubber Bearings for Earthquake Protection," *Rubber World*, 202(4), (April).

Hwang, J. S, and Ku, S.W. [1997] "Analytical modelling of high damping rubber bearings*" Journal of Structural Engineering*,123(8), (August).

Kelly, J. [1988] *Earthquake Resistant Design with Rubber*, Department of Civil Engineering, University of Chile (Textbook).

Mata, P. And Boroschek, R. [2001] "Caracterización mecánica de goma de alto amortiguamiento para el desarrollo de disipadores de energía," *2º Congreso iberoamericano de ingeniería sísmica.* 10-16 Oct, Madrid, Spain.

Mata, P. Boroschek, R. and Barbat, A. [2005] "Desarrollo de un modelo fenomenológico para una goma de alto amortiguamiento aplicada a disipadores de energía," *International Center for Numerical Methods in Engineering, (CIMNE), Earthquake Engineering Monograph.* (In press).

Mata, P. Boroschek, R. and Barbat, A. [2004] "Analytical model for high damping elastomers applied to energy dissipating devices. Numerical study and experimental validation," *Proceedings of the Third European Conference on Structural Control*, 3ECSC, Vienna, Austria.

Moroni, M. Sarrazín, R. and Boroschek, R. [1988] "Experiments on a Base Isolated Buildings in Santiago, Chile," *Engineering Structures*, 20(8), 720 –725.

Naeim, F. and Kelly, J. [1999] "Design of seismic isolated structures. From theory to Practice," (Jhon Wiley & Sons, Inc).

Salomón, O. Oller, S. and Barbat, A. [1999] "Modelo numérico de elastómeros multi-fase y su aplicación a estructuras con aislamiento sísmico," *Monografía CIMNE IS-36*, Technical University of Catalonia, UPC.

SAP [2004] *CSI Analysis Reference Manual for SAP2000, ETABS and SAFE.* Computer and Structures Inc. 1995 University Avenue, Berkeley, California USA.

Sarrazín, M. Moroni, M. and Boroschek, R. [1993] "Experiments on a Base Isolated Confined Masonry Buildings," *Proceedings ATC, 17-1 Seminar on Seismic Isolation, Passive Energy Dissipation, and Active Control*, Vol. 1, San Francisco.

Sommer, J. G. [1989] "Effect of Shape and Other Design factors on Rubber Behaviour," *Rubber World*. 201(3) (December).

Soong, T. T. and Dargush, G. F. [1997] "*Passive Energy Dissipation System in Structural Engineering*," (John Wiley & Sons, Inc., New York).

Sues, R. H. Mau, S. T. and Wen, Y. K. [1988] "System Identification of Degrading Hysteretic Restoring Forces," *Journal of Engineering Mechanics.* 114(5).

Wen, Y. K. [1976] "Method for Random Vibration of Hysteretic Systems," Journal of the Engineering Mechanics Division. ASCE, 102(2), 249-263.

Wilson, E. L. [1998] "Three Dimensional Static and Dynamic Analysis of Structures, a Physical Approach with Emphasis on Earthquake Engineering," *Computers and Structures, Inc.* Berkeley, California, USA.

Valles, R. E. Reinhorn, M. Kunnath, S. K. Li, C. and Madan, A. [1996] "IDARC-2D, A program for inelastic Damage Analysis of Buildings", Technical Report NCEER 96-00-10. National Centre for Earthquake Engineering Research.